

Deformation of soft clay ground under Raft foundation with consideration of influence parameters when the groundwater level changes at different depths

Thy TRUC DOAN^{1,4}, Hien HO THU^{1,3}, Thang NGUYEN DANH^{2,3}*

¹ University of Science, Ho Chi Minh City, Vietnam, 227 Nguyen Van Cu, Cho Quan Ward, Ho Chi Minh City, Vietnam

² University of Technology, Ho Chi Minh City, Vietnam, 268 Ly Thuong Kiet, Dien Hong Ward, Ho Chi Minh City, Vietnam

³ Vietnam National University, Ho Chi Minh City, Vietnam, Dong Hoa Ward, Ho Chi Minh City, Vietnam

⁴ Kien Giang University, Vietnam, 320A- 61 Highway, Vinh Hoa Hiep, Chau Thanh District, An Giang Province, Vietnam

* Corresponding email: dtthy@vnkgu.edu.vn

Abstract: *In recent decades, previous research has been done on the displacement of the soft ground under the raft foundation by many methods such as experiments in the laboratory, simulation, and field from many countries in the world. However, the measurement of the influence parameters (cohesion, current Young's modulus E , active pores pressure, passive pores pressure) of the soft clay ground when the groundwater level changes at different depths wasn't done particularly. So this research uses the finite element method (PLAXIS 3D software) and experiments in the laboratory to evaluate, analyze, and calculate the results of deformation (displacement) of the soft clay ground under the raft foundation when considering the influent parameters (cohesion, current Young's modulus E , active pores pressure, passive pores pressure) of the soft clay ground when the groundwater level changes at different depths). The research results clearly show that the value of cohesion parameters with the different groundwater levels at the depths affecting the deformation (displacement, settlement) of the soft clay ground is significant. Moreover, the other influent parameters such as Current Young's modulus, and active and passive pores pressure changes make remarkable differences in the deformation (displacement, settlement) when the groundwater level changes at different depths. Finally, in the above analyses, it is essential and urgent to research the deformation of the clay ground where the soil is located under the seawater levels variations at depths, and the ground is always affected by saltwater intrusion under the raft foundation where there is no research for this deformation. Moreover, the research results supply useful references to the field of scientific research on Geotechnics, construction, engineers, scientists, lecturers, students, and experts to use these research results to reduce and save labor, survey time, calculation... in the work of surveying, designing and constructing foundations on weak clay soil in the future.*

Keywords: *Cohesion; Current modulus Young; Active pore pressure; Passive pore pressure; Deformation (displacement or settlement); Groundwater levels; Depths*

1. Introduction

In recent decades, research on the raft foundation behaviors has been done in many methods which include experiments, simulations, fields, etc. The research results related to the settlements, deformation, shear strength, pore water pressure, optimal loading capacity, ground shapes, etc. Moreover, the evaluation of the deformation of the circle foundation on the sand ground behaviors with consideration of the N_c , N_q , and N_γ and other affections to the radius, smooth, and rough foundation. The results presented in the foundation settlement are remarkable (Amin K and Jayant K, 2017). In addition, the research on the affection of oil-contaminated sand to the square foundation capacity. The results described in percentage of oil variations reduced on the sand ground according to the reduced local shear failure as the polluted sand layer at the depths (Ahmed et al., 2019). Moreover, a small-scale model test was used to evaluate the comprehensively optimal settlement ratio when the wide 'B' and distance 'S' of the foundation ratio ($S/B = 0.7\%$). The percentage of loading capacity reach to 39%. Results show a reduced settlement of 0.7% of the raft foundation according to the maximum pile length (Elwakil and Azzam, 2016). Moreover, a small-scale model test was done to evaluate the comprehensively optimal settlement ratio when the wide 'B' and distance 'S' of the foundation ratio ($S/B = 0.7\%$). Results show the reduced settlement of 0.7% of the raft foundation according to the maximum pile length (Elwakil and Azzam, 2016). In addition, the pile-raft foundation settlements were measured with the nonlinear behavior of pile groups. (Hung and Jiang, 2011). In the other hand, the small-scale physical model of the pile and raft has been done to survey the

displacement ‘settlement’ at two stages. Results show that loading is less than 70% resulting in the lower ultimate capacity of piles (Hoang and Matsumoto, 2020). In the other hand, the shape factors for circular footings were used to evaluate footing bearing capacity. Results presented that the factors s_q and s_c are big when the friction angle (ϕ) is big (Loukidis D and Salgado R, 2009). Moreover, Results demonstrated that the different soil properties resulted in the different settlements (Lee et al., 2010). From the above discussion, it is essential to do the research on the raft foundation settlement and the vertical displacement with the consideration of groundwater level (depths) variations and the affective parameters that include Cohesion forces, Young modulus E, active pore pressure, passive pore pressure with the depths. A combination method is used in this research that shows experimental and simulation measurements by the ‘PLAXIS 3D software – finite element method’.

2. Geological background

This research presents the deformation (or settlement or displacement) of the ground under the Raft foundation when considering some affected parameters. The clay ground has always been covered fully by the seawater level variations. The clay soil particles are filled with water, which creates a buoyant force that will push the particles further apart, leading to the binding force between the soil particles weakening, easily breaking, and the particles will be separated easily and move in the water environment. When the raft foundation loading increased remarkably the load-bearing capacity of the soil was weaker than that causing the remarkable displacement and settlement of the ground. Especially, the big loading of the raft foundation affected the ground resistance with related parameters such as cohesion force, Young’s modulus, and so on. Therefore, to clear consideration of the clay ground behaviors under the raft foundation settlement (or displacement). The research measured the experimental tests in the laboratory and simulation of the Plaxis 3D software to give out essential, reliable, and exact results to the references in Geology engineering in the future. . .

3. Methodology

3.1 Materials

Clay soil with marine origin is sieved to remove impurities and kept moist for 24 hours at room temperature 26°C. Depths of the groundwater levels from 0.0m to 30.0m. A total of **48 samples** were collected at 4 boreholes. The standards used to measure this research Vietnam Standards ‘TCVN 4202:2012 - Soils - Laboratory methods for determination of units unit of unit weight’, ‘TCVN 4200:2012 - Soil – Laboratory methods for determination of compressibility’, ‘TCVN 4199:2012 - Soil - Laboratory method of determination of shear resistance in a shear box apparatus’.

3.2 The experiment measurement to determine the Cohesion Forces with the Depths

The Undrained – Unconfined Consolidation Test (UUCT) was done with 48 samples. The samples are kept moist within 24 hours. The soil samples are put in the sample box (size 60x60mm). The cutting speed reaches to 0.005mm/ minute. The Loading set up 0.25 kg/cm²; 0.5 kg/cm²; 1.0 kg/cm²; 1.25 kg/cm²; 1.5 kg/cm²; 2.0 kg/cm²; 3.0 kg/cm²; 4.0 kg/cm².

3.3 The experiment measurement to determine the Young’s modulus E with the Depths

The Undrained–Unconfined Consolidation Test (UUCT) was done at the lowest speeds to measure the settlement and strains of 48 samples after 24 hours for each sample. Loading us set up 0.25 kg/cm²; 0.5 kg/cm²; 1.0 kg/cm²; 2.0 kg/cm²; 4.0 kg/cm²; 8.0 kg/cm². Young’s Modulus parameters are done by the formula below:

$$E = \sigma / \zeta \text{ (kN/m}^2\text{)} \quad (1)$$

Whereas E is Young’s modulus (or plastic modulus of the soil)

σ is stress (kN/m²)

ζ is strain (constant)

3.4 Model simulation parameters assumptions

a) Ground, the Raft foundation structure parameters, Mesh, and Calculation stages

The finite element method (the PLAXIS 3D software) simulation is based on the Mohr-Coulomb theory. The basic parameters of the model are shown in Table 2 and Figure 1. The building parameters are shown in Table 3. The Clay ground depths (groundwater levels) from 0.0m to 40.0m. Mesh is divided into the full model with very small elements which supports to calculation full model’s areas more exactly. There are three calculating stages for the raft foundation loading. The first stage shows no loading, only soil ground loading. The second stage shows active loading with soil ground and plate ‘raft foundation slab’. The third

stage presents the loading active with full parameters such as soil, plate ‘raft foundation slab’, beam, wall, and coulomb. The building wall is 50cm reinforcement concrete thickness. The floor loadings are transmitted to the slabs through the beam and column systems. The concentrated loads on columns are 11650 kN with connection of the walls 385 kN/m. The soil ground stiff $E' = 5000 \text{ kN/m}^2$ and this value increases by 500 kN/m^2 per meter of depth. The groundwater levels are set up at 0.5m; 1.0m; 2.0m; 2.5m; 3.0m; 3.5m; 4.0m; 5.0m; 5.5m; 6.5m; 7.5m; 8.5m; 9.5m; 10.0m; 12.0m; 14.0m; 16.0m; 18.0m; 20.0m; 22.0m; 24.0m; 26.0m; 28.0m; 30.0m depths (see table 1 and figure 1).

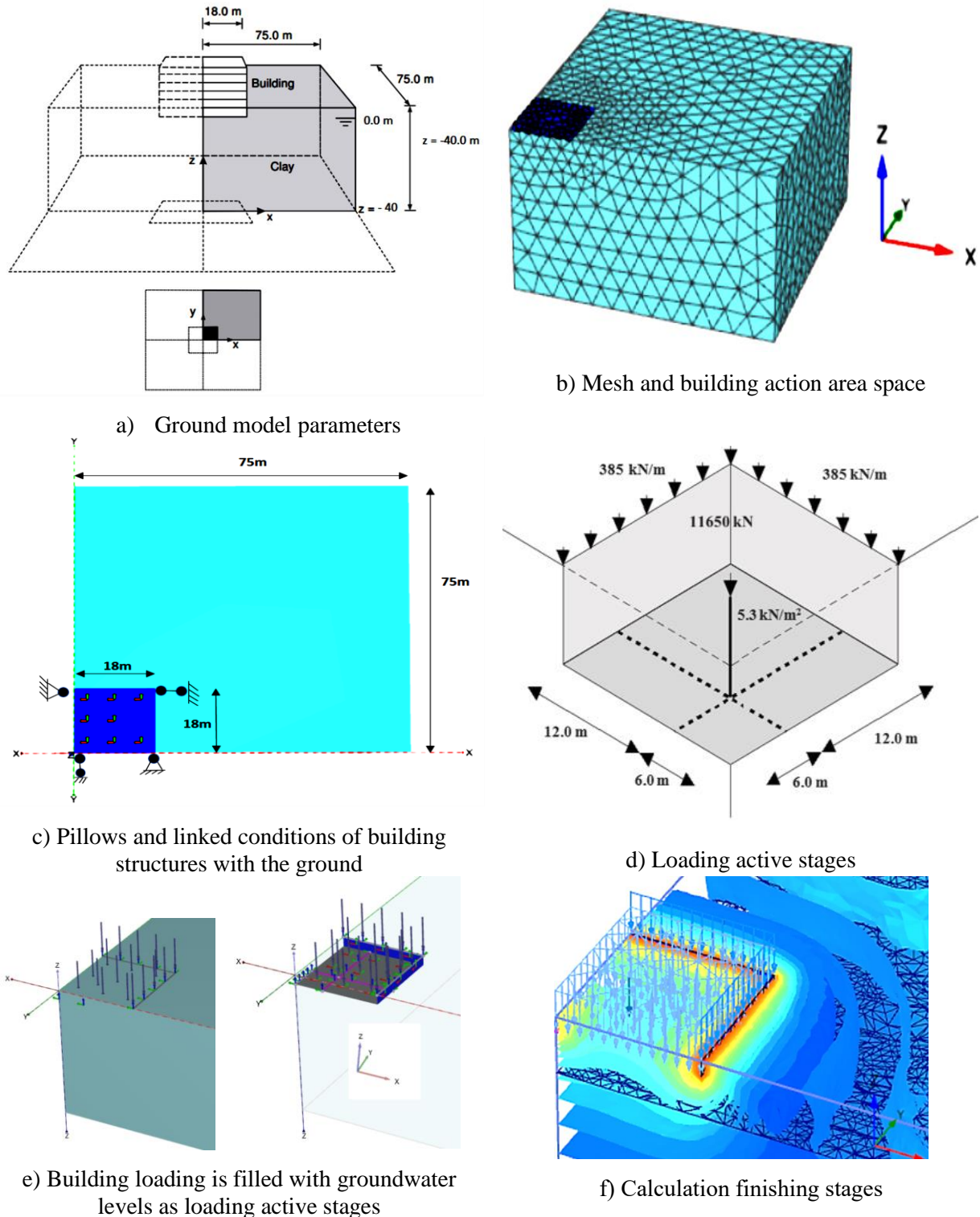


Fig. 1. Model calculation parameters

Tab. 1. Model simulation parameters assumptions (Thy Truc Doan, 2024)

Descriptions	Signs	Value	Unit
Soil ground properties			
Unit weight above the groundwater level	γ_{usat}	18.2	kN/m^3
Unit weight above the groundwater level	γ_{sat}	18.79	kN/m^3
Young's modulus (constant)	E'	Changes with the different depths	kN/m^2
Poisson's ratio	ν'	0.3	-
Maximum Cohesion (constant)	C'_{ref}	Changes with the different depths	kN/m^2
Lateral earth pressure coefficient	K_0	0.5	-
Structure properties			
Stiffness	$\nu'_{(\text{nu})}$	0.3	-
Type of behaviors	-	Linear, isotropic	kN/m^2
Thickness	d	-	m
Weight	γ	50	kN/m^3
Young's modulus	E_1	3.10^7	kN/m^2
Poisson's ratio	ν_{12}	0.15	-

4. Results

4.1 Experimental results

4.1.1 Results of the Relationship between the Maximum Cohesion Force and Depths from 2.5m to 30.3m

The Maximum Cohesion Force and Depths are calculated particularly from the experimental data from 2.5m to 30.3m depths. Results recorded that the maximum Cohesion forces values 45 kN/m^2 ; 40 kN/m^2 ; 37 kN/m^2 ; 40 kN/m^2 ; 56 kN/m^2 ; 53 kN/m^2 ; 59 kN/m^2 ; 54 kN/m^2 ; 42 kN/m^2 ; 32 kN/m^2 ; 38 kN/m^2 ; 32 kN/m^2 with 2.5m; 5.8m; 7.8m; 10.3m; 12.8m; 15.3m; 17.8m; 20.3m; 22.8m; 25.3m depths of the groundwater levels. (see figure 2). However, the strains are big when the big pore size distribution and the remaining curve continuedly (Arroyo H et al., 2015). The Tsunami caused a big pore water pressure that resulted in big sediment ground deformation (Abdollahia. A. and Mason H. B, 2019). The inclinometer sensors show the embankment displacements are remarkable when the increasing of lateral displacements increases as the platform distance decreases. Some longitudinal cracks appeared along the sides of the embankment (Acosta L. et al., 2019). Moreover, a coupled computational fluid dynamics-discrete element method (CFD-DEM) was used to measure the flow velocity. Results presented that the fine particles are small (Arumugam. H et al., 2023).

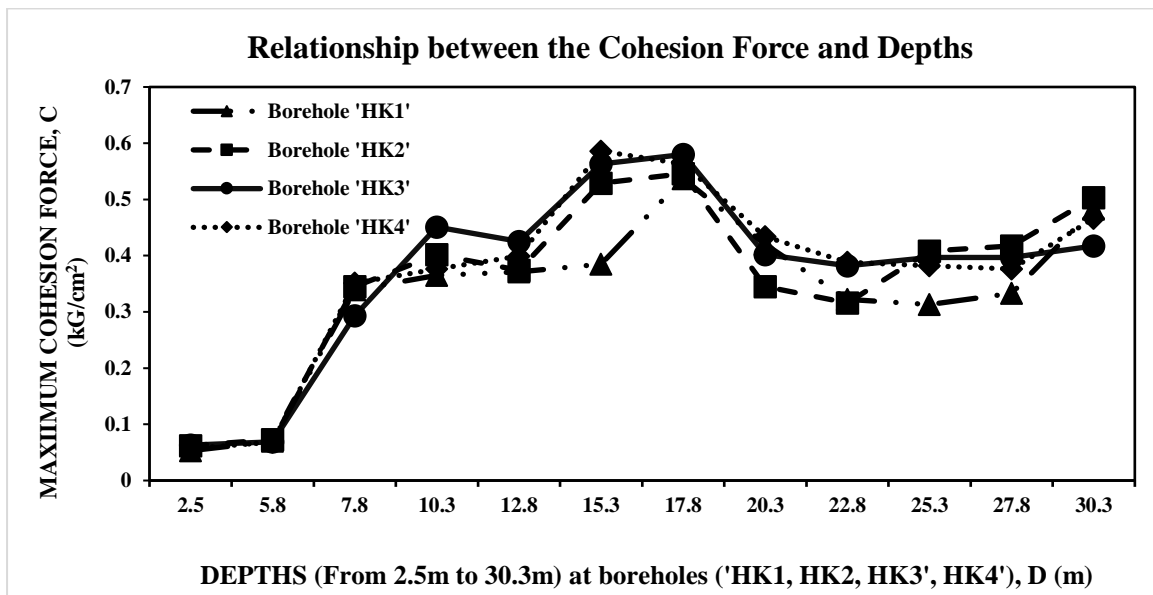


Fig. 2. Relationship between the Maximum Cohesion Force and Depths from 2.5m to 30.3m

4.1.2 Results of the relationship between Maximum Cohesion Forces and Depths from 0.0m to 50.0m

The calculation values can be interpolated with the bigger depths from 0.0m to 50.0m by the 'Origin 2024B' software. The results show the maximum Cohesion forces values 7.0 kN/m²; 45.1 kN/m²; 56.3 kN/m²; 54.6 kN/m²; 38.8 kN/m²; 48.3 kN/m²; 46.6 kN/m² with 0.0m; 4.7m; 9.4m; 14.1m; 18.8m; 23.5m; 28.2m depths of the groundwater levels. (see figure 3). However, the results presented time is big with the flow is big (Binh et al., 2022). The compressive loading is big and results in a high surface settlement of 4 m in 1390 days (Chai et al., 2010). The settlement measured at 14.5m towards the end of the combined loadings and the settlement curves converged (Chu and Yan, 2015). Additionally, the bearing pressure and footing structural resistance are high according to the soil-structure interaction impact (Cristiano G and Lyesse L, 2021).

4.1.3 Results of the Relationship between the Cohesion Forces, Vertical Displacements, and Depths from 9.5m to 25.3m

The remarkable results present that the maximum displacement values of the Clay ground obtained 0.0233 cm; 0.1652 cm; 0.1592 cm; 0.1685 cm; and 0.2082 cm according to the loading account for 0.5 kG/cm²; 1.0 kG/cm²; 2.0 kG/cm²; 4.0 kG/cm²; 8.0 kG/cm² and the maximum depths such as 19.8m; 20.3m; 9.6m; and 22.3m of the different groundwater levels. The other results are shown in figure 4 (see figure 4). However, the initial foundation shapes increased gradually when the friction angle was big (Cao. D et al, 2014). The Boundary Element Method (BEM) and the Finite Element Method (FEM) presented the relationship between plate-soil-pile and the stiffness matrix that resulted in the big settlement (Endi and João, 2019).

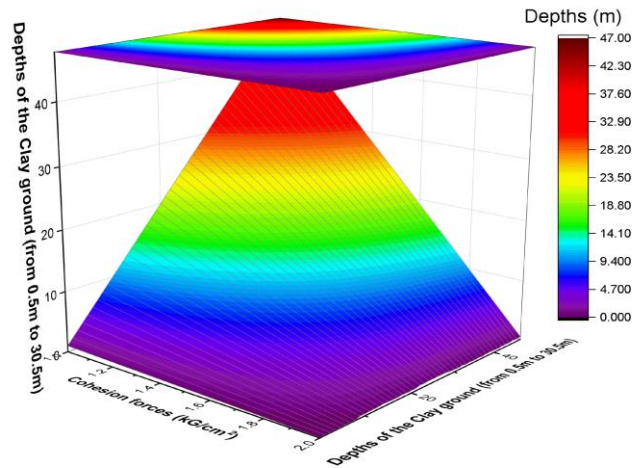


Fig. 3. The relationship between Cohesion Forces and Depths of the Clay ground at 0.0m to 50.m

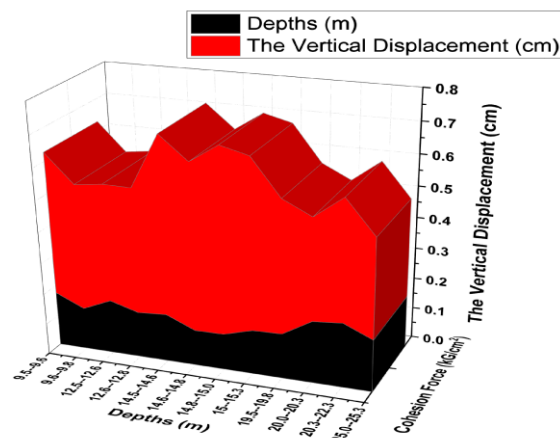


Fig. 4. The relationship between the Cohesion Forces, Depths, and Vertical Displacements

However, the fine particle soil and the glass fibers were 0%, 5%, 10%, 15%, 20% and 25%. The water-cement accounted for 0.55% which resulted in lower stress with the optimal loading (Elrahmani. H et al., 2022). The structure deformation is broken when the propagation of the micro-particle and the remarkable loading curves vary (Edem. I. E et al., 2022). However, the ground settlement reached 0.5m with the 4 vibration compactions (Feng et al., 2014). The foundation deformation changed with the groundwater changed gradually (Gazetas, 1981). the influences of freeze-thaw (FT) cycles and saline intrusion affected to the big shrinkage (Gaetano. G et al., 2022). The ground slope deformation decreased when the flow-independent viscosity, time, and soil factors increased (Hui L et al., 2021).

4.1.4 Results of the Relationship between the Load, Depths, and Vertical Displacements

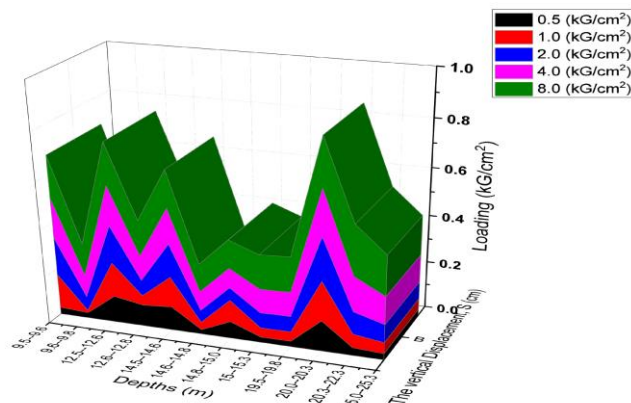


Fig. 5. The relationship between the Load, Depths, and Vertical Displacements

4.1.5 Results of the Relationship between the Young’s Modulus E, Depths, Cohesion Forces, and Vertical Displacements

The Young’s Modulus E values are determined by the Unconfined Compression Test of 48 samples after 24 hours at different depths from 0.0m to 30.3m. The highest value of the vertical displacement (settlement) reached **0.2082 cm** with Young’s modulus E of **141.2 kG/cm²** with the Cohesion forces of **0.38 kG/cm²** at **22.3m** depth. On the other hand, the other values are shown in figure 6. (see figure 6). However, the permeability coefficient of bentonite is small with bentonite of the deep layers at 25⁰C; 100⁰C and 105⁰C temperatures (Hongbo L et al., 2022). with a membrane-less vacuum consolidation technique combined with a loading system 50 kPa suction (MS24). The lateral displacement is reduced in a suction head (Indraratna et al., 2018). The slip surface of the ground reduced gradually when the friction angle reached 300⁰C (James J et al, 2022).

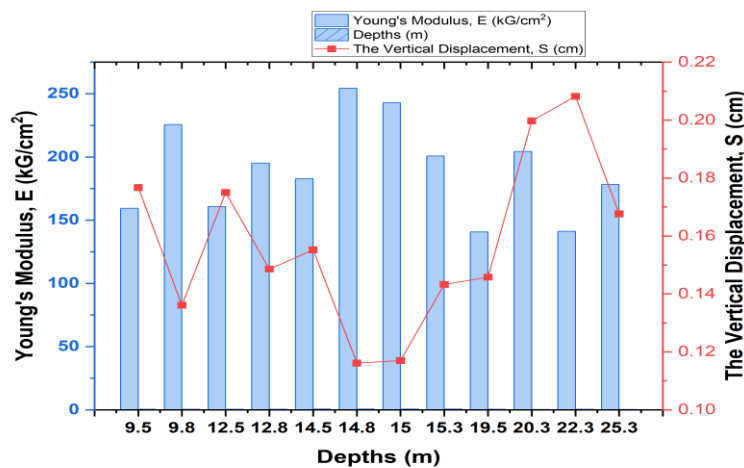


Fig. 6. The relationship between Young’s Modulus E, Depths, Cohesion Forces, and Vertical Displacements

There is no affection of the structure where the reinforcement structure located in the many chloride environments according to the Chloride diffusion coefficients appeared in greater density (Jianhe. X et al., 2022).

4.2 Simulation results

4.2.1 Results of the relationship between the Cohesion Forces, Vertical displacements, and Depths

The maximum vertical displacement value shows **4.348x10⁻³ m** at **0.5m** of the lowest depth with a Cohesion force of **4.1 kN/m²**, and the maximum vertical displacement value increased gradually to **4.946x10⁻³ m** at **30.0m** depth with a maximum Cohesion force of **46.725 kN/m²**.

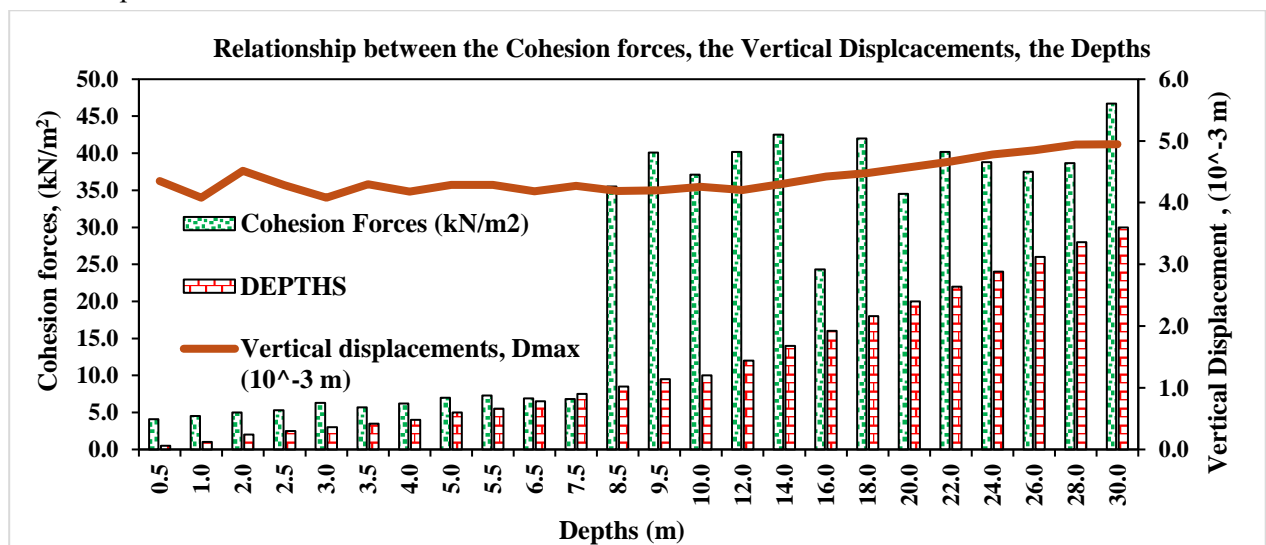


Fig. 7. The relationship between the Cohesion Forces, Vertical displacements, and Depths

The raft foundation settlement was affected by the different soil conditions, number of stories, number of bays, the ratio of flexural stiffness of columns, beams, ground excitation frequency, and seismic factor (Koushik et al., 2004). The displacement of the vacuum pile system of the peat layer according to the low embankments/overburden (Kelly 2014). The clay ground settlement remarkably and reduced the risks of staged construction of embankments (Krishnapriya et al., 2016). The bearing capacity of strip footing reached 87.7% when e/B values from 0 to 1/3 for $\alpha = 0^\circ$ of the effect of inclined and eccentric loads (Krishnan. K and Chakraborty. D, 2022).

4.2.2 Results of the relationship between Young’s modulus E, Vertical displacements, and Depths

Results presented that the maximum displacement (settlement) values 15.9×10^{-3} m at 25.3 m depth according to Yung’s modulus E of 141.2 kN/m^2 . The highest value of the vertical displacement (settlement) reached 15.65×10^{-3} m at 22.3m depth compared with the lower value of Young’s modulus E of 225.55 kN/m^2 at 9.8m depth. (see Figure 8). However, the load-sharing model and centrifuge load tests demonstrated that the ratio of loading sharing decreased (Lee et al., 2014). Moreover, the maximum inward lateral displacement appeared at the lower shallow depth near the ground surface (Long et al., 2015). Two models soil-water (FD) and element finite (FE) show the lower surface settlement, horizontal displacement, and pile group when a large extent (Linlin G. et al., 2020). With particle diameter D50 and the void ratio being constant, the C_u value is bigger (Liu X et al., 2021).

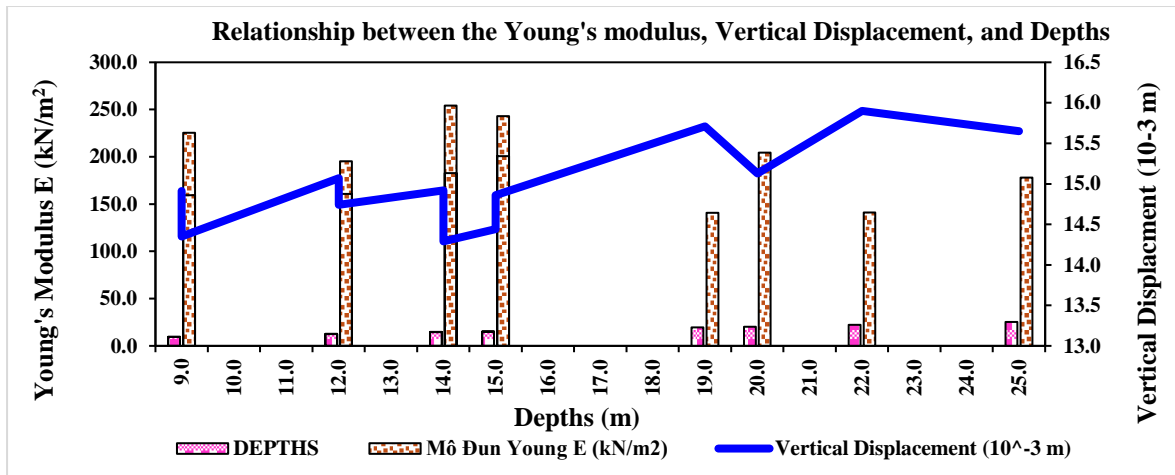


Fig. 8. The relationship between the Young’s modulus E, Vertical displacements, and Depths

4.2.3 Results of the Relationship between the Passive (Steady) pores pressure, Vertical displacements, and Depths

At 30.0m depth, the vertical displacement obtained 4.946×10^{-3} m with the lowest value of passive (steady) pore pressure of 0 kN/m^2 that compared with the maximum value of the passive (steady) pore pressure is 295 kN/m^2 with 4.348×10^{-3} m of the vertical displacement at 0.5m depth (see Figure 9). However, the foundation surface was set up at a large friction angle of the granular soil ground (Leila A. L. N et al, 2022). The volumetric strains were deformed by the suction or stress variations of an expansive bentonite/silt mixture. Result in the increased suction swelled soil with no loading (Lin. J et al., 2022). The surface settlement is shown in the upper 8 m soft clay ground at 2, 5, 8, 12, and 16 m depths (Moh and Lin, 2005). The Vertical Displacement of the Circular Foundation on the over-consolidation Ground shows the low displacement with the big loading (Thy T. D, 2022).

4.2.4 Results of the Relationship between Active Pores Pressures, Cohesion Forces, and Depths

At 25.3m depth, the lowest value of active pore pressure of 47 kN/m^2 with the Cohesion force is 33.3 kN/m^2 ; compared with the maximum value of the active pore pressure is 205 kN/m^2 with the Cohesion force is 45.1 kN/m^2 at 9.5m depth (see Figure 10).

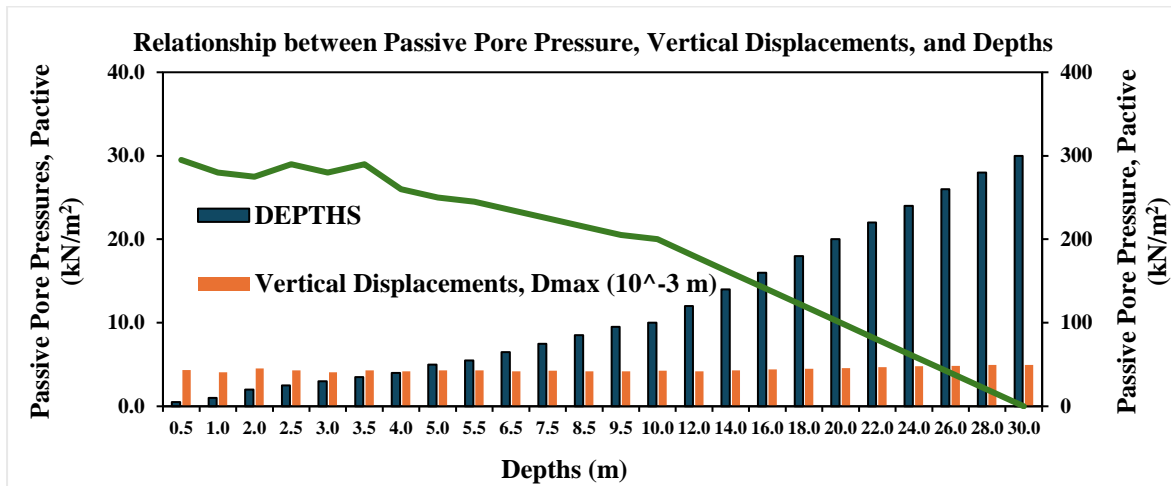


Fig. 9. The Relationship between the Passive (Steady) pores pressure, Vertical displacements, and Depths. However, surface settlement in 250 days is 1.0m as vacuum preloading at 5m depth (Nguyen et al, 2015). Finite element analysis results evaluated the side force that was affected by the internal friction angle influence (Ozaki. S and Kondo. W, 2016). The highest drying stress increased after drying stress increased (Rućknagel. J et al., 2007). Ilwis Software and Kriging Interpolation to Simulate 3D Stratigraphic Structure Model described the clay ground with cohesion forces, colors, thickness, and physical characteristics (Thy T. D, 2022).

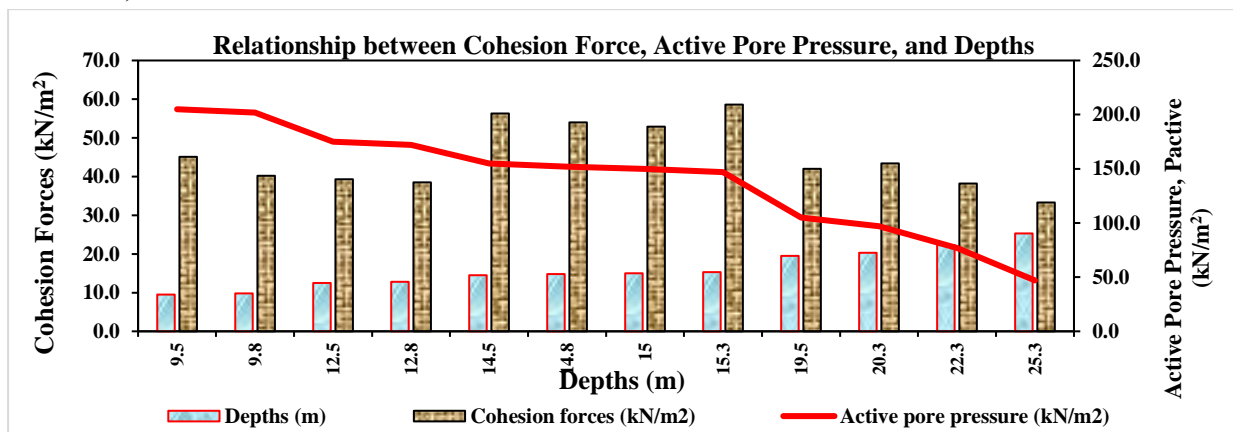


Fig. 10. The Relationship between Active pores pressure, Cohesion Forces, and Depths

4.2.5 Results of the relationship between Active pores pressure, Cohesion Forces, and Vertical Displacements

Moreover, the vertical displacements of the ground obtained a maximum value of 17.27×10^{-3} m according to the lowest active pore pressure values of 47 kN/m^2 whereas the relative Cohesion force is 33.3 kN/m^2 ; On the contrary, when the depth increased gradually, that results in the vertical displacement reduced gradually of 16.18×10^{-3} m with the maximum active pore pressure values of 205 kN/m^2 whereas the relative Cohesion force is 45.1 kN/m^2 ; (see Figure 11). However, the results described the dissipation of excess pore water pressure and the slow development of settlement after 12 hours and the high and low interface resistance of about 78.3% (Wang et al., 2016). The stable dissipation values of the pore water pressure were -55.2, -55.9, -60.7, -63.2, -68.3, and -52 kPa (Wang J et al., 2019). The Clay Ground under the Rigid Foundation displaced particularly at the different depths (Thy T. D, 2023).

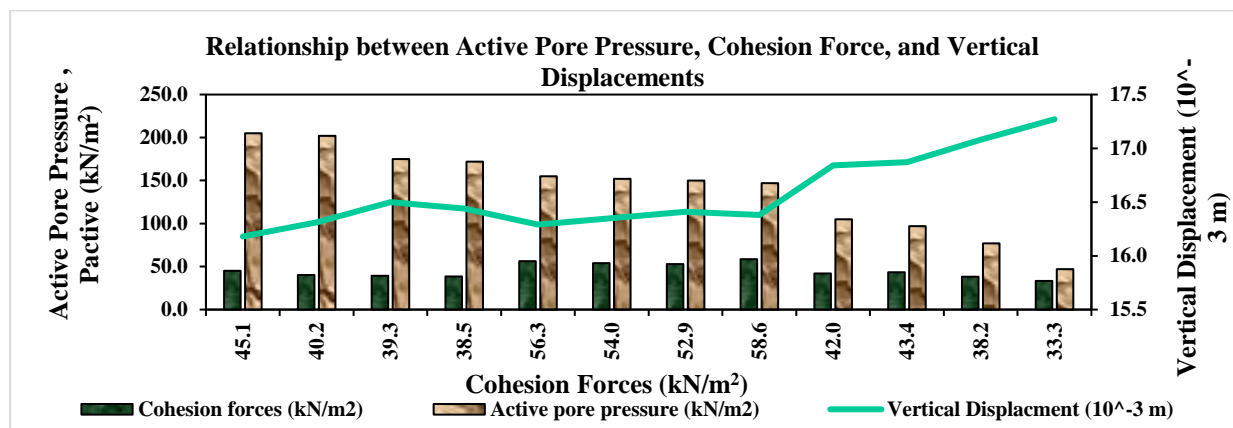


Fig. 11. The Relationship between Active pores pressure, Cohesion Forces, and Vertical Displacements

5. Discussion

The reasonable advice on decreasing the environmental influence found a improve the vacuum preloading workcraft (Yan et al., 2010). The maximum ground surface settlements were -77 mm, -68 mm, -122 mm, and -120 mm with the help of electro-osmotic consolidation and the maximum lateral displacement was supported by 4 devices (Zhang and Hu, 2018). the cracks in the Sodium Chloride concentration and temperature changes (Thy T. D, 2024) chemical components in water affect concrete structure with the depths (Thy T. D, 2024). Shear Resistance Variations With the different groundwater level variations at the Depths, the ground settlement is low values (Thy T. D, 2023). the groundwater levels variations affect to the vertical displacement of the clay ground (Thy T. D, 2023). Research results show shear stress ' τ ' according to the shear displacement ' Δl ' with different dry densities for deep reconstituted soils and the shear strength decreases sharply (Xiao-dong. Z et al., 2009). Effects of gravel content and shape on the shear behavior of soil-rock mixture made the increase of weak soil-gravel exceed 40% (Yao Y et al., 2022). The results presented ultimate inclined load per unit area depended on the H/B ratio and value $B'=B - 2e$ as the ratio B/H is constant (Sethy B. P et al., 2020). Equations that affected the permeability coefficient and no change and stability ground (Minghua. L et al., 2022).

6. Conclusion

From the above analysis, this research results evaluate the deformation of soft clay ground under raft foundation with consideration of influence parameters (cohesion, current Young's modulus e, active pores pressure, passive pores pressure) when the groundwater level changes at different depths particularly. Generally, the influence parameters affected by the vertical deformation of soft clay ground under raft foundation is a quite small change. Moreover, a combination of the experimental and simulation by the finite element method (PLAXIS 3D software) that show clearly that the active and passive pore pressure is the same at the same depths of the groundwater level variations that compared with cohesion forces and Young's modulus E are big changes at the different depths. Finally, the research results are reliable and useful data to refer to the scientific research on Geotechnics, construction, engineers, scientists, lecturers, students, and experts to use these research results to reduce and save labor, survey time, calculation, etc in the work of surveying, designing and constructing foundations on weak clay soil in the future.

Acknowledgments

Authors thank the anonymous reviewers for improving the paper.

Literature - References

1. Arroyo H, Eduardo R, Maria D. L. L. P, Jaime H, Arroyo J, 2015. A porous model to simulate the evolution of the soil–water characteristic curve with volumetric strains. J. Comptes Rendus Mécanique, 343 (4), 264 - 274. <http://dx.doi.org/10.1016/j.crme.2015.02.001>

2. Amin K. and Jayant K, 2017. Bearing capacity computation for a ring foundation using the stress characteristics method, *Computers and Geotechnics*, 89, 33-42. <https://doi.org/10.1016/j.compgeo.2017.04.006>
3. Abdollahia A, Mason H. B, 2019. Tsunami-induced pore water pressure response of unsaturated soil beds: Numerical formulation and experiments, *J. Computers and Geotechnics*, 110, 19 – 27. <https://doi.org/10.1016/j.compgeo.2019.02.012>
4. Acosta L. N. P, Santiago E. A. L, Núñez P. V. M, Ossa A, Mendoza M. J, Shelley O. E, Botero E, 2019. Performance of a test embankment on very soft clayey soil improved with rain-to-drain vacuum preloading technology, *J. Geotextiles and Geomembranes*, 47 (5), 618-631. <https://doi.org/10.1016/j.geotexmem.2019.103459>
5. Ahmed I. F. A. A. I. F, Mohammed. Y. F, 2019. Bearing capacity of isolated square footing resting on contaminated sandy soil with crude oil, *Egyptian Journal of Petroleum*, 28 (3), 281-288. <https://doi.org/10.1016/j.ejpe.2019.06.005>
6. Arumugam H, Iqbal M. M, Hee C, Ahn R. S, Muthukaruppan A, 2023. Development of high-performance granite fine fly dust particle reinforced epoxy composites: structure, thermal, mechanical, surface, and high voltage breakdown strength properties. *J. Materials research and technology*, 24, 2795 - 2811. <https://doi.org/10.1016/j.jmrt.2023.03.199>
7. Binh T. N, Tatsuya I, Yulong Z, Srikrishnan S. S, Thanh T. N, 2022. New simplified transient method for determining the coefficient of permeability of unsaturated soil, *Engineering Geology*, 300, 106 - 564. <https://doi.org/10.1016/j.enggeo.2022.106564>
8. Chai J, Hong Z, Shen S, 2010. Vacuum- drain consolidation induced pressure distribution and ground deformation, *J. Geotextiles and Geomembranes*, 28, 525 -535. <https://doi.org/10.1016/j.geotexmem.2010.01.003>
9. Chu J, Yan S, 2015. Application of the Vacuum Preloading Method in Soil Improvement Projects, Elsevier Geo-Engineering Book Series, 3, 91 – 117. [https://doi.org/10.1016/S1571-9960\(05\)80006-0](https://doi.org/10.1016/S1571-9960(05)80006-0)
10. Cristiano G. and Lyesse. L, 2021. Soil-structure interaction of surface footings, *Computers and Geotechnics*, 134, 104 – 103. <https://doi.org/10.1016/j.compgeo.2021.104103>
11. Dang D. C. N, Seong. B. J, Dong. S. K, 2013. Design method of piled-raft foundations under vertical load considering interaction effects, *Computers and Geotechnics*, 47, 16– 27. <https://doi.org/10.1016/j.compgeo.2012.06.007>
12. Dingfeng C, Sanjay K. S, Linqing Y, Chengchao G, Jinghong W, Fuming W, 2014. Responses of calcareous sand foundations to variations of groundwater table and applied loads, *Journal of Rock Mechanics and Geotechnical Engineering*, 14 (4), 1266 – 1279. <https://doi.org/10.1016/j.jrmge.2021.08.003>
13. Elwakil A. Z and Azzam W. R, 216. Experimental and numerical study of piled raft system, *Alexandria Engineering Journal*, 55, 547 – 560. <https://doi.org/10.1016/j.aej.2015.10.001>
14. Endi S. L and João B. P, 2019. A 3D BEM/FEM formulation for the static analysis of piled rafts and capped pile groups subjected to vertical and horizontal loads, *Engineering Analysis with Boundary Elements*, 103, 66 – 79. <https://doi.org/10.1016/j.enganabound.2019.02.009>
15. Elrahmani A, Riyadh I, Raoush A, Abugazia H, Seers T, 2022. Pore-scale simulation of fine particle migration in porous media using coupled CFD-DEM. *J. Powder Technology*, 398, 117 – 130. <https://doi.org/10.1016/j.powtec.2022.117130>
16. Edem I. E, Jude. C. O, Victor E. I, 2022. Comparative study on recycled iron filings and glass particles as a potential fine aggregate in concrete, *J. Resources, Conservation & Recycling Advances*, 15, 200 – 093. <https://doi.org/10.1016/j.rcradv.2022.200093>
17. Feng J. S, Lu F. S, Shi M. Z, Shui H. W, 2014. Densification of loosely deposited soft soils using the combined consolidation method, *Engineering Geology*, 181, 169 - 179. <https://doi.org/10.1016/j.enggeo.2014.07.010>
18. Gazetas G, 1981. Variation estimation of the settlement of a circular raft on anisotropic soil, *Soils and Foundations*, 21 (4), 110 - 116. https://doi.org/10.3208/sandf1972.21.4_109
19. Gaetano G, Greco F, Leonetti L, Nevone B. P, Pascuzzo A, 2022. A hybrid cohesive/volumetric multiscale finite element model for the failure analysis of fiber-reinforced composite structures. *J. Procedia Structural Integrity* 41, 439 – 451. <https://doi.org/10.1016/j.prostr.2022.05.050>

20. Huang M, Liang F, Jiang J, 2011. A simplified nonlinear analysis method for piled raft foundation in layered soils under vertical loading, *Computers and Geotechnics* 38, 875 – 882. <https://doi.org/10.1016/j.compgeo.2011.06.002>
21. Hoang L. T, Matsumoto T, 2020. Long-term behavior of piled raft foundation models supported by jacked-in piles on saturated clay, *Soils and Foundations*, 60, 198 – 217. <https://doi.org/10.1016/j.sandf.2020.02.005>
22. Hui L, Yunzhi T, Ziyang X, De S, Wenjing S, 2021. Method for measuring the saturated permeability coefficient of compacted bentonite at temperatures exceeding 100°C, *Progress in Nuclear Energy*, 141, 103 - 958. <https://doi.org/10.1016/j.compgeo.2022.104763>
23. Hongbo L, Guoliang D, Fengxi Z, Xiaolin C, Liye Wang, 2022. Effect of flow-independent viscosity on the propagation behavior of Rayleigh wave in partially saturated soil based on the fractional standard linear solid model, *J. Computers and Geotechnics*, 147, 104 - 763. <https://doi.org/10.1016/j.pnucene.2021.103958>
24. Indraratna B, Rujikiatkamjorn C, Baral P, Ameratunga J, 2019. Performance of marine clay stabilized with vacuum pressure: Based on Queensland experience, *J. Rock Mechanics and Geotechnical Engineering*, 11 (3), 598 - 611. <https://doi.org/10.1016/j.jrmge.2018.11.002>
25. James J, King D, Roberts T, Joe A. C. Bruce K. L, 2022. Numerical modelling of the growth of polygonal fault systems, *Journal of Structural Geology*, 104 - 679. <https://doi.org/10.1016/j.jsg.2022.104679>
26. Jianhe X, Junjie W, Molan L, Lei X, Dong X, Yuli W, Hang H, Yi Z, Jinxia Z, 2022. Estimation of chloride diffusion coefficient from water permeability test of cementitious materials, *J. Construction and Building Materials*, 340, 127 – 816. <https://doi.org/10.1016/j.conbuildmat.2022.127816>
27. Koushik B, Dutt S. C, Dasgupta. S, 2004. Effect of soil - flexibility on dynamic behaviour of building frames on raft foundation, *Journal of Sound and Vibration*, 274, 111–135. [https://doi.org/10.1016/S0022-460X\(03\)00652-7](https://doi.org/10.1016/S0022-460X(03)00652-7)
28. Kelly O'.C. B, 2015. Case studies of Vacuum Consolidation Ground Improvement in Peat Deposits, *Ground Improvement Case Histories Embankments with Special Reference to Consolidation and Other Physical Methods*, 315 – 345. <https://doi.org/10.1016/B978-0-08-100192-9.00011-9>
29. Krishnapriya P. B, Sandeep M. N, Antony J, 2016. Efficiency of Vacuum Preloading on Consolidation Behaviour of Cochin Marine Clay, In proceeding of 24th International Conference on Emerging Trends in Engineering, *Procedia Technology*, 24, 256 -262. <https://doi.org/10.1016/j.protcy.2016.05.034>
30. Krishnapriya P. B, Sandeep M. N, Antony J, 2016. Efficiency of Vacuum Preloading on Consolidation Behaviour of Cochin Marine Clay, In proceeding of 24th International Conference on Emerging Trends in Engineering, *Procedia Technology*, 24, 256 -262. <https://doi.org/10.1016/j.protcy.2016.05.034>
31. Krishnan K, Chakraborty D, 2022. Probabilistic study on the bearing capacity of strip footing subjected to combined effect of inclined and eccentric loads, *Computers and Geotechnics* 141, 104505. <https://doi.org/10.1016/j.compgeo.2021.104505>
32. Loukidis D, Salgado R, 2009. Bearing capacity of strip and circular footings in sand using finite elements, *Computers and Geotechnics*, 36 (5), 871-879. <https://doi.org/10.1016/j.compgeo.2009.01.012>
33. Lee J, Youngho K, Sangseom J, 2010. Three-dimensional analysis of bearing behavior of piled raft on soft clay, *Computers and Geotechnics*, 37, 103 – 114. <https://doi.org/10.1016/j.compgeo.2009.07.009>
34. Lee J. P. D, Choi K, 2014. Analysis of load sharing behavior for piled rafts using normalized load response model, *Computers and Geotechnics*, 57, 65 – 74. <https://doi.org/10.1016/j.compgeo.2014.01.003>
35. Long P. V, Nguyen L. V, Bergado D. T, Balasubramaniam A. S, 2015. Performance of PVD improved soft ground using vacuum consolidation methods with and without airtight membrane, *J. Geotextiles and Geomembranes*, 43 (6), 473-483. <https://doi.org/10.1016/j.geotexmem.2015.05.007>
36. Linlin G, Zhen W, Qiang H, Guanlin Y, Feng Z, 2020. Numerical investigation into ground treatment to mitigate the permanent train-induced deformation of pile-raft-soft soil system, *Transportation Geotechnics*, 24, 100 - 368. <https://doi.org/10.1016/j.trgeo.2020.100368>

37. Liu X, Degao Z, Jingmao L, Bowen Z, 2021. Predicting the small strain shear modulus of coarse-grained soils, *J. Soil Dynamics and Earthquake Engineering*, 141, 106 – 468. <https://doi.org/10.1016/j.soildyn.2020.106468>
38. Leila A. N, Seyedeh. H. F, Meghdad. P, Reza J. C, Ali S, 2022. Interaction of rigid shallow foundation with dip-slip normal fault rupture outcrop: effective parameters and retrofitting strategies, *Computers and Geotechnics* 149, 104866. <https://doi.org/10.1016/j.compgeo.2022.104866>
39. Lin J, Zou W, Han Z, Zhang Z, Wang X, 2022. Structural, volumetric, and water retention behaviors of a compacted clay upon saline intrusion and freeze-thaw cycles. *J. Rock Mechanics and Geotechnical Engineering*, 14, 953 - 966. <https://doi.org/10.1016/j.jrmge.2021.12.012>
40. Moh C. Z, Lin P, 2005. Case Study of Ground Improvement Work at the Suvarnabhumi Airport of Thailand, Elsevier Geo-Engineering book series, chapter 3, volume 3, 159 - 198. [https://doi.org/10.1016/S1571-9960\(05\)80009-6](https://doi.org/10.1016/S1571-9960(05)80009-6)
41. Minghua L, Baiquan L, Wei Y, Yang Z, Zheng W, 2022. In-situ testing method of the permeability coefficient in a coal seam based on the finite volume method and its application, *J. Natural Gas Science and Engineering*, 97, 104 - 370. <https://doi.org/10.1016/j.jngse.2021.104370>
42. Nguyen S. H, Tashiro M, Inagaki M, Yamada S, Noda T, 2015. Simulation and evaluation of improvement effects by vertical drains/vacuum consolidation on peat ground under embankment loading based on a macro-element method with water absorption and discharge functions, *J. Soils and Foundations*, 55(5), 1044 - 1057. <https://doi.org/10.1016/j.sandf.2015.09.007>
43. Ozaki S, Kondo W, 2016. Finite element analysis of tire traveling performance using anisotropic frictional interaction model, *Journal of Terramechanics* 64, 1–9. <https://doi.org/10.1016/j.jterra.2015.12.001>
44. Rućknagel J, Hofmann B, Paul R, Christen O, Huřlsbergen K. J, 2007. Estimating pre-compression stress of structured soils based on aggregate density and dry bulk density. *J. Soil & Tillage Research*, 92, 213 – 220, <https://doi.org/10.1016/j.still.2006.03.004>
45. Sethy B. P, Patra C.R, Das B. M, Sobhan. K, 2020. Behavior of circular foundation on sand layer of limited thickness subjected to eccentrically inclined load, *Soils and Foundations*, 60 (1), 13 – 27. <https://doi.org/10.1016/j.sandf.2019.12.005>
46. Thy Truc Doan, 2024. Experiment measurement of the cracks by the Sodium Chloride concentration and temperature changes, *J. Materials Today Proceedings*. <https://www.sciencedirect.com/science/article/abs/pii/S2214785324000877>
47. Thy Truc Doan, 2024. Comprehensive Evaluation of the aggressive certain degree of the chemical components in water to concrete, *Front. Built Environ, Sec. Construction Materials*, Vol 10. <https://www.frontiersin.org/articles/10.3389/fbuil.2024.1275218/full>
48. Thy Truc Doan, 2023. Comparison between Numerical Analysis and Experiment for the Dry Density and Shear Resistance Variations with the different Depths (groundwater level variations), *J. Geology, Ecology, and Landscapes*. <https://www.tandfonline.com/doi/full/10.1080/24749508.2023.2254011>
49. Thy Truc Doan, 2023. Finite Element Method of the Internal friction angle and Saturation Degree with the groundwater levels variations. *J. Geology, Ecology, and Landscapes*, 7 (4), 429-450. <https://www.tandfonline.com/doi/full/10.1080/24749508.2023.2202426?src=recsys>.
50. Thy Truc Doan, 2022. Three (3d) Dimension Model of Settlement Differences of the Clay Ground Under Rigid Foundation by The Affection of the Groundwater Variations – A Comparison. The 2nd International Conference on Civil and Environmental Engineering (ICCEE 2022), Malaysia. *J. E3S Web of Conferences*, 1, 347. <https://www.e3sconferences.org/component/solr/?task=results#!q=thy%2Btruc%2Bdoan&sort=relevance&rows=10>
51. Thy Truc Doan, 2022. The Application of Geostatistical Software (SGeMS), Ilwis Software, and Kriging Interpolation to Simulate 3D Stratigraphic Structure Model Urban Rach Gia town, Kien Giang Province, Viet Nam. The 2nd International Conference on Civil and Environmental Engineering (ICCEE 2022), Malaysia, *J. E3S Web of Conferences*, 1. 347. <https://www.e3sconferences.org/component/solr/?task=results#!q=thy%2Btruc%2Bdoan&sort=relevance&rows=10>.
52. Thy Truc Doan, 2022. Evaluation of the Vertical Displacement of the Circular Foundation on the over-consolidation Ground in Phu Quoc Island, Kien Giang Province, Viet Nam. The 6th Conference on

- Civil Engineering for Sustainable Development, India (ICCEE 2022), Khulna, Bangladesh, India. http://103.157.135.50/proc_2022/Papers/GTE-01125.pdf
53. Wang J, Ma J, Liu F, Mi W, Cai Y, Fu H, Wang P, 2016. Experimental study on the improvement of marine clay slurry by electroosmosis-vacuum preloading, *J. Geotextiles and Geomembranes*, 44, 615 - 622. <https://doi.org/10.1016/j.geotexmem.2016.03.004>
 54. Wang J, Huang G, Fu H, Cai Y, Hu X H, Lou X, Jing Y, Hai J, Ni J, Zou J, 2019. Vacuum preloading combined with multiple-flocculant treatment for dredged fill improvement, *J. Engineering Geology*, 259, 105 - 194. <https://doi.org/10.1016/j.enggeo.2019.105194>
 55. Xiao Z, Zhou G, Tian Q, 2009. Study on the shear strength of deep reconstituted soils, *J. Mining Science and Technology*, 19 (3), 0405 – 0408. [https://doi.org/10.1016/S1674-5264\(09\)60076-4](https://doi.org/10.1016/S1674-5264(09)60076-4)
 56. Yao Y, Jue L, Junjun N, Chenghao L, Anshun Z, 2022. Effects of gravel content and shape on shear behavior of soil-rock mixture: Experiment and DEM modelling. *J. Computers and Geotechnics*, 141, 104 – 476, <https://doi.org/10.1016/j.compgeo.2021.104476>
 57. Yan J, Wang Q, Zhang J, 2010. Environmental Influence of Vacuum Preloading Dredging Project, *Procedia Environmental Sciences*, 2, 1613 - 1621. <https://doi.org/10.1016/j.proenv.2010.10.172>
 58. Zhang L, Hu L, 2018. Laboratory tests of electro-osmotic consolidation combined with vacuum preloading on kaolinite using electrokinetic geosynthetics, *J. Geotextiles and Geomembranes*, 47, 166 - 176. <https://doi.org/10.1016/j.geotexmem.2018.12.010>
 59. *Standards
 60. Vietnam Standard ‘TCVN 4202:2012 - Soils - Laboratory methods for determination of unit weight’.
 61. Vietnam Standard ‘TCVN 4200:2012 - Soil – Laboratory methods for determination of compressibility’.
 62. Vietnam Standard ‘TCVN 4199:2012 - Soil - Laboratory method of determination of shear resistance in a shear box apparatus’.